Aminopolycarboxylate Bismuth(III)-Based Heterometallic Compounds as Single-Source Molecular Precursors for Bi 4 V 2 O 11 and Bi 2 CuO 4 Mixed Oxides

Ion Bulimestru, Sergiu Shova, Nelea Popa, Pascal Roussel, Frédéric Capet, Rose-Nöelle Vannier, Nora Djelal, Laurence Burylo, Jean-Pierre Wignacourt, Aurelian Gulea, et al.

Aminopolycarboxylate Bismuth(III)-Based Heterometallic Compounds as Single-Source Molecular Precursors for $Bi_4V_2O_{11}$ and Bi_2CuO_4 Mixed-Oxides

Ion Bulimestru[1], Sergiu Shova[2], Nelea Popa[1], Pascal Roussel[3], Frederic Capet[3], Rose-Noelle Vannier[3], Nora Djelal[3], Laurence Burylo[3], Jean-Pierre Wignacourt[3], Aurelian Gulea[1] and Kenton H. Whitmire[4]

[1] Moldova State University, Coordination Chemistry Laboratory, 60 Mateevici str., Chisinau MD 2009, Moldova

[2] Institute of Macromolecular Chemistry "Petru Poni", Aleea Gr. Ghica Voda 41A, 700487, Iasi, Romania

[3] Université Lille Nord de France, Unité de Catalyse et de Chimie du Solide, CNRS UMR 8181, ENSC Lille – UST Lille, BP 90108, 59652 Villeneuve d'Ascq cedex, France

[4] Department of Chemistry, MS 60, Rice University, 6100 Main Street, Houston, Texas 77005

ABSTRACT

Five heterometallic complexes of general formula $M(L)_y\{Bi(APC)\}_2 \cdot nH_2O$ ($M = VO^{2+}$, Cu^{2+}; APC = aminopolycarboxylate - in this work ethylenediaminetetraacetate ($edta^{4-}$) or 1,2-cyclohexanediaminetetraacetate ($cdta^{4-}$); L = 2,2'-bipyridine; y = 0, 1 or 2; n = 5 – 16) have been synthesized. The crystal structures of four of them have been determined from single crystal X-ray diffraction data. The compounds have been probed as single-source molecular precursors for $Bi_4V_2O_{11}$ and Bi_2CuO_4 mixed-oxides. Temperature controlled X-ray powder diffraction was used to monitor the phase transitions during the thermolysis of the precursors. The influence of the ligand type and intermetallic distances in the precursors, heating rate and the atmosphere have been investigated. The best candidates to yield pure $Bi_4V_2O_{11}$ and Bi_2CuO_4 are complexes with separations between hetero-metals of ~4 Å containing ~29-30% of carbon. The optimal working conditions under which the precursors can be smoothly converted to the corresponding heterometallic oxides are heating at low rates under air flow. The precursors containing ~29-30% of carbon yield smaller grains and more homogeneous morphology of the residues than the analogues with lower or higher carbon amount. The advantage of the APC-based molecular precursor method is compared to previously reported procedures to produce bimetallic oxides.

KEY WORDS: heterometallic complexes, bismuth, vanadyl, copper, aminopolycarboxylate, ionic conductor, mixed-oxides.

INTRODUCTION

The increasing demand for devices designed for high-tech applications requires nanomaterials of uniform morphology and detailed knowledge of the reaction processes that lead to preparation of the desired products. Among the main targets are heterometallic oxides that exhibit a more complex array of optical, magnetic and electronic properties compared to their homometallic analogues. Some of the properties might be combined within the same compound giving access to multifunctional materials such as multiferroics.[1]

With respect to physical characteristics that are important for advanced technology, a major target has become multimetallic bismuth(III) oxides due to their broad spectrum of potential applications including the next generation of data storage devices,[2] high T_c superconductors,[3] solid electrolytes,[4] nonlinear optical and luminescent materials,[5] selective oxidation catalysts[6] and photocatalysts.[7] Apart from their valuable physical properties, bismuth-containing materials have elicited considerable interest due to their potential environmentally benign alternatives to cadmium- or lead-based thermochromic systems[8] or as "green" lubricants.[9] Among the heterometallic Bi(III)-based oxides, bismuth vanadate, $Bi_4V_2O_{11}$ has been extensively examined for its fascinating ionic conducting behavior,[10] as well as for its dielectric, pyroelectric and ferroelectric properties.[11] The ionic conductivity, catalytic performance and mechanical resitance of $Bi_4V_2O_{11}$ can be considerably enhanced by partial substitution of the vanadium(V) ion by other metallic cations leading to the so called BIMEVOX family of heterometallic oxides.[12] On the other hand, bismuth cuprate, Bi_2CuO_4 is the parent compound for producing high-temperature Bi-Cu-M-(M')-O superconductors.[13] Additionally, bismuth-copper oxides have been investigated as efficient catalysts in different processes.[14]

The performance of many oxide materials has been reported to be sensitive to the synthesis conditions.[15] The multimetallic oxides are traditionally prepared by the ceramic route, which generally requires long heating times at high temperatures as well as repeated grinding. Consequently, this method does not always yield single-phase products of the desired stoichiometry and granularity. When high-tech materials and devices with dimensions on the nanometer scale are concerned, more sophisticated synthetic pathways such as chemical vapour deposition,[16] mechanochemical activation,[17] hydrothermal methods,[18] sol-gel[19] or ionic layer deposition[20] are better choices.

An alternative synthetic strategy to tune the stoichiometry and microstructure of the oxide materials is the single-source molecular precursor (SSMP) method.[21] This route not only allows an intimate mixing of the different metal species on an atomic scale but considerably reduces the diffusion distances of the reactants and, as a consequence, the reaction time and temperature. The achievements in the field of SSMP method for the formation of Bi-based oxide materials have been summarised.[22] Ideally, a SSMP contains the exact ratio of the required metal atoms corresponding to the stoichiometry of the desired oxide. However, the synthesis of heterometallic compounds often represents an ambitious challenge because of the frequently divergent electronic and coordination requirements of the different metal species. These problems are further exacerbated when bismuth-containing compounds are involved, due to bismuth's high tendency to hydrolyze. As a result, the structural information available for heterometallic complexes of bismuth is relatively limited. However, an examination of the structures of the precursors could give some insight of the relationship between the intermetallic separations, thermal behaviour and composition of the resulting oxide materials.

Different routes to the formation of discrete heterobimetallic bismuth-based coordination complexes, mainly with alkoxide or carboxylate ligands, have been reported.[23] We have examined the ability of aminopolycarboxylic (H_xAPC) acids (x = 3-5) to control the hydrolysis process and to associate two different metal centres in a desired ratio within a heterobimetallic compound. The most attractive features of H_xAPC chelating agents are their high coordination capacity and variable charge which afford an easy adjustable stoichiometry of the target metals. Moreover, upon thermal treatment, APC-based precursors release large amounts of gaseous products favoring the formation of porous materials that are of utmost importance in catalysis. Along this line, we have started a systematic investigation of the influence of homologues APC ligands on the thermal degradation processes of heterometallic precursors and on the composition and microstructure of the final residue. The nature of the APC ligand is responsible for crystal packing and intermetallic distances that might affect the mixed-oxide formation process. Moreover, changing the organic matrix in the starting compounds can result in different morphological properties of the final oxide materials regarding the particle's shape and size, specific surface area and porosity.[24] Our previous work on the Ba-Co-containing system[25] demonstrated that, among the molecular precursors with the same Ba:Co ratio and similar APC ligands (nta^{3-} = nitrilotriacetate, $edta^{4-}$ = ethylenediaminetetraacetate, $cdta^{4-}$ = 1,2-cyclohexanediaminetetraacetate, $dtpa^{5-}$ = diethylenetriaminepentaacetate), only the $cdta^{4-}$-containing complexes led to pure 2H-$BaCoO_{3-\delta}$ upon thermal treatment at 650ºC. In this context we have expanded our studies to the formation of $Bi_4V_2O_{11}$ and Bi_2CuO_4 mixed oxides by thermolysis of appropriate molecular precursors based on different APC ligands. The major objective has been to elucidate the factors that would lead to pure heterometallic oxides of uniform morphology and nano-sized grains.

A rational method for the synthesis of heterobimetallic APC complexes with Bi:M = 2:1 ratio was targeted to achieve the metal stoichiometry in the desired mixed-oxides. This flexible synthetic pathway has proven efficient in the preparation of $BaCo^{II(III)}$(APC) molecular precursors.[25] Considering this, we have synthesized five coordination compounds of general formula $M(L)_y\{Bi(APC)\}_2 \cdot nH_2O$ ($M = VO^{2+}$, Cu^{2+}; APC = $edta^{4-}$ or $cdta^{4-}$; L = 2,2'-bipyridine; y = 0, 1 or 2; n = 5-16) and used them as single-source molecular precursors for $Bi_4V_2O_{11}$ and Bi_2CuO_4 heterometallic oxides. The decomposition behaviour of the precursors has been studied by combined TG/DTA. The complexes were heated in static air to produce oxide-residues. Temperature controlled X-ray powder diffraction (TCXRD) has been performed under static or flowing air at different heating rates to elucidate the possible differences in phase transitions during thermolysis of the precursors. Scanning electron microscopic (SEM) studies were carried out to give some indication of grain size and morphology of the product particles at the final stage of the thermal treatment.

EXPERIMENTAL SECTION

General. H_4edta, H_4cdta·H_2O, KOH, $BaCO_3$, $Bi(NO_3)_3 \cdot 5H_2O$, $CuSO_4 \cdot 5H_2O$ and $VOSO_4 \cdot 3H_2O$ were obtained from Sigma-Aldrich and 2,2'-bipyridine was purchased from Fluka. All reagents were used without any further purification. Microanalysis (C, H, N) was performed with a Vario EL(III) elemental analyzer. Infrared spectra of the complexes were recorded on a Perkin Elmer 100 FT-IR instrument in 600-4000 cm^{-1} range using ATR methodology with a ZnSe window.

TGA measurements were carried out with a SETARAM 92-1600 instrument. The samples (4-10 mg) were heated in platinum crucibles to 600°C at a 10 °C·min^{-1} rate under static air.

X-ray thermodiffractometry (TCXRD) studies were carried out using an ENRAF Nonius Guinier-Lenné moving film camera (heating rate 0.2 °C min^{-1}, 58h exposure, film speed 2 mm·h^{-1}, static air) or a D8 Bruker AXS powder diffractometer, equipped with a Ni filter, a VANTEC™ PSD detector and an Anton Paar HTK1200N high temperature device (heating rate 10 °C·min^{-1}; static air or air flow, 5 L·h^{-1}). A diagram was recorded every 25 ^{o}C in the 10-70° 2θ domain. Both X-ray methods used Cu Kα (λ = 1.54187 Å) radiation. The precursors were deposited on platinum or gold sample holders (grid or thin foil) as thin layers using ethanol slurry that yields a regular layer of the powdered sample upon evaporation.

The inorganic residues, obtained upon thermal treatment of the precursors, were examined at room temperature by powder X-ray diffraction with a Huber G670 diffractometer with Guinier geometry, equipped with front-monochromator using CuKα_1 radiation (λ =1.54056 Å) or with a D8 Bruker AXS diffractometer using CuKα radiation (λ =1.54187 Å), equipped with a Sol-X energy dispersive detector.

The microstructural properties of the resulted residues were characterized using a FEG Hitachi Ltd. S-4700 Scanning Electron Microscope (SEM).

Single crystal X-ray Crystallography. Crystallographic measurements for **1**, **2** and **4** were carried out on Oxford-Diffraction XCALIBUR E CCD diffractometer and on Bruker SMART APEXII CCD diffractometer for **5** equipped with graphite-monochromated Mo-Kα radiation.

Table 1. Crystallographic data, details of data collection and structure refinement parameters for **1, 2, 4** and **5**.

	1	**2**	**4**	**5**
Empirical formula	$C_{40}H_{94}N_8O_{57}Bi_4V_2$	$C_{60}H_{128}N_{12}O_{66}Bi_4V_2$	$C_{28}H_{57.4}N_4O_{27.7}Bi_2V$	$C_{28}H_{46}N_4O_{21}Bi_2Cu$
Formula weight	2537.03	3011.54	1362.28	1256.19
Temperature/K	200	200	293	100
Crystal system	monoclinic	triclinic	triclinic	triclinic
Space group	*C*2/*c*	$P\bar{1}$	$P\bar{1}$	$P\bar{1}$
a/Å	27.5715(10)	13.7503(5)	11.344(5)	7.3231(1)
b/Å	14.034(3)	14.6200(7)	15.095(5)	8.6724(1)
c/Å	21.883(2)	14.8330(6)	16.393(5)	14.6870(2)
α/°	90.00	109.239(4)	65.746(5)	94.234(1)
β/°	91.279(5)	100.299(3)	72.998(5)	95.056(1)
γ/°	90.00	107.386(4)	77.854(5)	107.973(1)
V/Å^3	8465.5(18)	2556.35(18)	2434.3(15)	878.75(2)
Z	4	1	2	1
D_{calc}/mg/mm^3	1.991	1.956	1.859	2.374
μ/mm^{-1}	8.606	7.149	7.488	10.685
Crystal size/mm^3	0.20×0.20×0.20	0.20×0.10×0.10	0.2×0.15×0.15	0.17×0.15×0.10
$2\theta_{min,}$ $2\theta_{max}$(°)	5.58 to 52	4.9 to 52.74	5.88 to 52	5.44 to 52.74
Reflections collected	26550	42345	15315	13865
Independent reflections	8645 [R_{int} = 0.0546]	10438 [R_{int} = 0.0449]	8105 [R_{int} = 0.0816]	3541 [R_{int} = 0.0249]
Data/restraints/ parameters	8645/0/489	10438/0/637	8105/72/561	3541/1/262
R_1[a](I>2σ(I)	0.0399	0.0519	0.0586	0.0155
wR_2[b](all data)	0.0998	0.1413	0.1183	0.0361
GOF[c]	1.050	1.058	1.003	1.089
Largest diff. peak/hole/e Å^{-3}	1.64/-2.01	3.29/-1.15	2,85/-2.67	0.76/-0.94

[a] $R_1 = \Sigma||F_o| - |F_c||/\Sigma|F_o|$, [b] $wR_2 = \{\Sigma[w\,(F_o^2 - F_c^2)^2]/\Sigma[w(F_o^2)^2]\}^{1/2}$.
[c] GOF = $\{\Sigma[w(F_o^2 - F_c^2)^2]/(n-p)\}^{1/2}$, where n is the number of reflections and p is the total number of parameters refined.

The single crystals were positioned at 40 mm from the detector. The unit cell determination and data integration of **1**, **2** and **4** were carried out using the CrysAlis package of Oxford Diffraction[26] and the APEX2 package of Bruker AXS for **5**. The structures were solved by direct methods using Olex2 software[27] with the SHELXS structure solution program and refined by full-matrix least-squares on F² with SHELXL-97.[28] Atomic displacements for non-hydrogen atoms were refined using an anisotropic model. All H atoms attached to carbon were introduced in idealized positions (d_{C-H} = 0.96 Å) using the riding model with their isotropic displacement parameters fixed at 120% of the riding atom. The molecular plots were obtained using the Olex2

program. The main crystallographic data together with refinement details are summarized in Table 1. X-ray crystallographic file (CIF) for **1**, **2**, **4** and **5** contains the supplementary crystallographic data for this contribution. This material is available free of charge via the Internet at http://pubs.acs.org.

Synthesis of the precursors

Method I. *[{VO(H$_2$O)$_3$}$_2${Bi(edta)}$_4$]·17H$_2$O* **(1)**. An aqueous solution of Ba{Bi(edta)}$_2$ (20 mL) was prepared by gradual reaction of $BaCO_3$ (0.197 g, 1 mmol) with Bi(Hedta)·2H$_2$O[29] (1.068 g, 2 mmol) with heating and continuous stirring. To this solution was added $VOSO_4$·3H$_2$O (0.217 g, 1 mmol) dissolved in 10 mL of distilled water. The precipitated $BaSO_4$ was removed by filtration. The resulting reaction mixture was concentrated to 2-3 mL at 40^{o}C and kept at -10^{o}C for 3 hours. Small prismatic light-blue crystals deposited from the solution at room temperature in three days. Yield: 0.81 g (~ 64 %). Anal. Calcd (%) for $C_{40}H_{94}N_8O_{57}Bi_4V_2$: C, 18.94; H 3.73; N4.42. Found (%): C, 18.89; H 3.70; N 4.40. FTIR (selected bands, cm^{-1}): 3233 (m vbr), 2975 (m br), 1562 (vs), 1432 (sh), 1408 (s), 1251 (m), 1380 (s), 1333 (s), 1319 (s), 1111 (vw), 1086 (w), 1041 (w), 958 (m), 914 (m), 881 (w), 851 (w), 809 (vw), 724 (w).

[{VO(bpy)(H$_2$O)}$_2${Bi(edta)}$_4$]·30H$_2$O **(2)**. To 15 mL of aqueous solution obtained in a manner similar to **1,** after removing $BaSO_4$, was added 2,2'-bipyridine (0.16 g, 1 mmol) dissolved in 5 mL of ethanol. The resulting green solution was concentrated to ~7 ml at 40 ^{o}C. Ethanol was then added dropwise with vigorous stirring until the reaction mixture became slightly turbid. The solution cleared up with additional stirring. Rhomboidal light-violet crystals started to deposit from the solution in 10-20 minutes. Yield: 0.902 g (~ 60 %). Anal. Calcd (%) for $C_{60}H_{128}N_{12}O_{66}Bi_4V_2$: C, 23.93; H, 4.28; N, 5.58. Found (%): C, 24.12; H, 4.21; N, 5.61. FTIR (selected bands, cm^{-1}): 3381 (m vbr), 2971 (m br), 1574 (vs), 1435 (m), 1404 (s), 1378 (sh), 1329

(sh), 1313 (s), 1244 (m), 1097 (sh), 1088 (w), 1035 (w), 954 (m), 911 (m), 881 (w), 851 (w), 809 (vw), 724 (w).

VO(bpy)$_2${Bi(edta)}$_2$·5H$_2$O **(3)**. Solid 2,2'-bipyridine (0.16 g, 1 mmol) was added to 25 mL of aqueous suspension of **1** (0.61 g, 0.5 mmol). The mixture was stirred and heated until all the reagents dissolved completely. The resulting green reaction mixture was evaporated at 40 ^{o}C to dryness. Yield: 0.709 g (~ 97 %). Anal. Calcd (%) for $C_{40}H_{50}N_8O_{22}Bi_2V$: C, 32.82; H 3.44; N 7.66. Found (%): C, 33.03; H 3.34; N 7.82. FTIR (selected bands, cm^{-1}): 3371 (m vbr), 2970 (w br), 1575 (vs), 1444 (m), 1363 (s), 1314 (s), 1244 (m), 1092 (w), 1028 (w), 973 (w), 915 (m), 854 (w), 768 (m), 732 (w), 710 (sh).

{[VO(H$_2$O)$_3${Bi(cdta)}$_2$]·7.7H$_2$O}$_n$ **(4)**. This compound was prepared in a manner analogous to **1** with the substitution of Bi(Hcdta)·5H$_2$O (1.285 g, 2 mmol) for Bi(Hedta)·2H$_2$O.[30] The solution, obtained after the removal of $BaSO_4$, was left for crystallisation at room temperature. In 1-2 hours small prismatic light-blue crystals started to deposit from solution. Yield: 0.858 g (~ 63 %). Anal. Calcd (%) for $C_{28}H_{57.4}N_4O_{27.7}Bi_2V$: C, 24.68; H 4.25; N 4.11. Found (%): C, 24.55; H 4.49; N 3.86. FTIR (selected bands, cm^{-1}): 3356 (m vbr), 2958 (m br), 1640 (s), 1557 (vs), 1388 (s), 1322 (s), 1241 (m), 1099 (m), 1082 (m), 984 (m), 922 (m), 880 (m), 841 (w), 787 (w), 727 (m).

{[Cu(H$_2$O)$_2${Bi(cdta)(H$_2$O)}$_2$]·H$_2$O}$_n$ **(5).** Compound **5** was prepared in a manner analogous to **4** with the substitution of $CuSO_4$·5H$_2$O (0.250 g, 1 mmol) for $VOSO_4$·3H$_2$O. The resulting reaction mixture was heated on a water bath until light-blue needle-like crystals started to form. The quantity of the crystals increased upon cooling. Yield: 0.748 g (~ 60 %). Anal. Calcd (%) for $C_{28}H_{46}N_4O_{21}Bi_2Cu_4$: C, 26.77; H 3.69; N 4.46. Found (%): C, 26.81; H 3.60; N 4.38. FTIR (selected bands, cm^{-1}): 3368 (s vbr), 2921 (m br), 2863 (sh), 1670 (s), 1597 (vs),

1451 (w), 1427 (w), 1399 (m), 1376 (s), 1351 (sh), 1298 (s), 1237 (m), 1092 (m), 1077 (m), 1014 (w), 1000(w), 967 (w), 923 (m), 907 (m), 875 (m), 785 (w), 722 (m).

Method II (compounds **1, 4** and **5**). Either Bi(Hedta)·$2H_2O$ (0.53 g, 1 mmol) or Bi(Hcdta)·$5H_2O$ (0.64 g, 1 mmol) was dissolved in 30 mL of hot distilled water and freshly prepared vanadyl or copper(II) carbonate-based species were gradually added while heating and stirring until no more evolution of CO_2 was observed. The non-reacted carbonates were removed by filtration and the resulting reaction mixtures were treated afterwards in manners analogues to method I. Yields: 0.37 g (~60 %) **(1);** 0.50 g (~68 %) **(4)**; 0.47 g (~ 75 %) **(5)**.

RESULTS AND DISCUSSION

Preparation and structures of the precursors. Two synthetic methods were used to prepare the complexes. In the first one $Ba\{Bi(APC)\}_2$, obtained *in situ* by reacting stoichiometric amounts of $BaCO_3$ with aqueous solutions of Bi(Hedta)·$2H_2O$ or Bi(Hcdta)·$5H_2O$, was further reacted with the vanadyl or copper sulphates according to Equations (1) and (2):

$$2Bi(HAPC) + BaCO_3 = Ba\{Bi(APC)\}_2 + H_2O + CO_2\uparrow \quad (1)$$

$$Ba\{Bi(APC)\}_2 + VOSO_4 = VO\{Bi(APC)\}_2 + BaSO_4\downarrow \quad (2)$$

In the second route, aqueous solutions of Bi(HAPC) complexes were treated with freshly prepared vanadyl or copper carbonate species as per Equation (3):

$$2Bi(HAPC) + VOCO_3 = VO\{Bi(APC)\}_2 + H_2O + CO_2\uparrow \quad (3)$$

The elimination of insoluble $BaSO_4$ or gaseous CO_2 from the reaction mixtures facilitates the association between $\{M(H_2O)_n\}^{2+}$ cations and $\{Bi(APC)\}^-$ anions.

Both synthetic approaches rely on the utilization of the polydentate H_4APC acids to direct the stepwise introduction of the two different metal species into the final compound. Considering the strong hydrolysis tendency of Bi^{3+} ions and high stability of Bi(APC) comlexes[31], bismuth was the first to be introduced into H_4APC matrix to get Bi(HAPC) species. Here, we took advantage of the acid-base properties of the reagents to adjust the desired Bi:M stoichiometry. The complexes with one or two moles of 2,2'-bipyridine were synthesized from the reaction of **1** and the organic base in water or ethanol-water. Here 2,2'-bipyridine was involved as an ancillary ligand capable of affecting the crystal packing and the amount of combustible material in the precursors.

The results of X-ray diffraction studies of complexes **1**, **2**, **4** and **5** together with selected atomic numbering scheme are shown in Figures 1−4. Selected bond distances are listed in Table 2.

Table 2. Selected bond distances (Å) for **1, 2, 4** and **5**

1		**2**		**4**		**5**	
V1-O1*w*	2.174(5)	V1-O1*w*	2.108(6)	V1-O1*w*	1.992(9)	Cu1-O2*w*	1.961(2)
V1-O2*w*	2.039(4)	V1-N5	2.115(8)	V1-O2*w*	2.03(1)		
V1-O3*w*	2.012(5)	V1-N6	2.094(4)	V1-O3*w*	1.98(1)	Cu1-O7	1.976(2)
V1-O6	1.985(5)	V1-O6	1.983(6)[1]	V1-O12	2.027(8)[3]		
V1-O12	1.984(5)	V1-O12	1.994(6)[1]	V1-O14	2.15(1)	Cu1-O6[1]	2.390(2)
V1-O17	1.594(5)	V1-O17	1.618(6)	V1-O17	1.63(1)		
Bi1-O1	2.471(4)	Bi1-O1	2.485(6)	Bi1-O1	2.430(9)	Bi1-O1	2.420(2)
Bi1-O3	2.291(5)	Bi1-O3	2.321(6)	Bi1-O3	2.40(1)	Bi1-O3	2.295(2)
Bi1-O5	2.519(4)	Bi1-O5	2.529(6)	Bi1-O5	2.488(8)	Bi1-O5	2.423(2)
Bi1-O7	2.409(5)	Bi1-O7	2.369(6)	Bi1-O7	2.314(9)	Bi1-O7	2.505(2)
Bi1-N1	2.504(6)	Bi1-N1	2.553(7)	Bi1-N1	2.47(1)	Bi1-N1	2.430(2)
Bi1-N2	2.442(6)	Bi1-N2	2.469(7)	Bi1-N2	2.472(9)	Bi1-N2	2.485(2)
Bi1-O5[1]	2.904(4)	Bi1-O5	2.883(6)[1]	Bi1-O10	2.864(9)	Bi1-O6[1]	2.814(2)
Bi1-O11	2.839(4)	Bi1-O11	2.822(6)[1]	Bi1-O10	2.600(9)[1]	Bi1-O1*w*	2.595(2)
Bi1-O17[1]	2.636(4)	Bi1-O17	2.512(6)				
Bi2-O9	2.428(4)	Bi2 O9	2.361(6)	Bi2-O9	2.37(1)		
Bi2-O11	2.701(4)	Bi2 O11	2.767(6)	Bi2-O11	2.425(8)		
Bi2-O13	2.358(4)	Bi2 O13	2.345(6)	Bi2-O13	2.444(8)		
Bi2-O15	2.384(5)	Bi2 O15	2.485(6)	Bi2-O15	2.42(1)		
Bi2-N3	2.555(5)	Bi2 N3	2.557(7)	Bi2-N3	2.51(1)		
Bi2-N4	2.416(5)	Bi2 N4	2.444(7)	Bi2-N4	2.523(9)		
Bi2-O2	2.524(5)	Bi2 O2	2.580(6)	Bi2-O2	2.62(1)		
Bi2-O7[1]	2.711(5)	Bi2 O7	2.633(6)[1]	Bi2-O16	2.73(1)[2]		
Bi2-O1	3.038(4)	Bi2 O1	3.165(6)[1]				

Symmetry codes: [1]1.5 - *x*, 0.5 - *y*, 1 - *z* for **1;**[1]1 - *x*, 1 - *y*, 1 - *z* for **2;** [1] 2 - *x*, 1 - *y*, -*z*; [2] 2 - *x*, -*y*, 1 – *z*; [3] -1 + *x*, *y*, *z* for **4;** [1] *x*, -*y*, -*z*, [2]-1 + *x*, *y*, *z*; [3]-1 - *x*, -*y*, -*z* for **5**

To the best of our knowledge, compounds **1**, **2** and **4** are the first structurally characterized molecular precursors for $Bi_4V_2O_{11}$ mixed-oxide. The only previous report of a crystal structure of a bismuth-vanadium complex is $[Bi^{III}Cl_3OV^{V}(OC_2H_4OCH_3)_3]_2$.[32] Structures of three more heterometallic polyoxometalates containing bismuth and vanadium $H_3[\{Bi(dmso)_3\}_4V_{13}O_{40}]\cdot 4dmso$,[33] or bismuth, vanadium and other metals $((CH_3)_4N)_6Na_4[(VO(H_2O)_2)_2(WO_2)_2(BiW_9O_{33})_2]\cdot 18H_2O$[34] and $K_{11}H[(BiW_9O_{33})_3Bi_6(OH)_3(H_2O)_3V_4O_{10}]\cdot 25H_2O$[35] have been also published. Compound **5** is only the second example of a structurally characterized molecular precursor for Bi_2CuO_4 phase, the first one being $Cu\{Bi(edta)\}_2\cdot 9H_2O$.[36] Regarding the metals ratio, another potential precursor for the bismth cuprate can be $[Bi_2Cu(hfac)_8]$[37] (hfac = hexafluoroacetylacetonate). Noteworthy, complexes **1** and **2** are the first examples with coordinated V^{IV}=O group to bismuth centres though compounds with vanadyl donor bonds to tin,[38] lead,[38c] nickel[39] or barium[40] have been reported.

[{VO(H$_2$O)$_3$}$_2${Bi(edta)}$_4$]·17H$_2$O **(1)**. Compound **1** has a molecular crystal structure comprising a neutral hexanuclear complex $[\{VO(H_2O)_3\}_2\{Bi(edta)\}_4]$ (Fig. 1) and water as solvate molecules. The V^{IV} ion is six-coordinate with a slightly distorted octahedral environment. The almost planar equatorial plane of the coordination octahedron is formed by the oxygen atoms of two water molecules in *cis* positions and the oxygen atoms of bridging carboxylate groups. The apical sites are occupied by the vanadyl oxygen atom at 1.594(5) Å and by the oxygen atom of a water molecule at a considerably longer distance (2.174(5) Å). The O17-V-O1*w* angle is 179.9(2)°. As expected, the V=O bond length is shorter than other V–O bonds and falls well into the range of 1.56-1.63 Å for typical V^{IV}=O distances.[41] The V^{IV} ion is displaced at 0.308 Å from the mean equatorial plane towards the vanadyl oxygen atom.

Both Bi1 and Bi2 display a coordination number of nine. The coordination polyhedron of Bi1 is close to a monocapped square antiprism. It includes six atoms (2N+4O) provided by *edta*$^{4-}$ ligand, two bridging carboxylate oxygen atoms and the vanadyl oxygen atom. The Bi1-O17-V angle (137.0(2)^{o}) is consistent with a sp^2 hybridization of the vanadyl oxygen and a double bond V=O character.[38a,c] The coordination environment of the Bi2 atom can be characterized as a strongly distorted monocapped square antiprism which comprises both O1 and O2 oxygen atoms of the carboxylate group coordinated as tridentate-bridging ligand. The Bi-O and Bi-N distances in **1** are similar to that reported for the analogous Bi-APC complexes.[31]

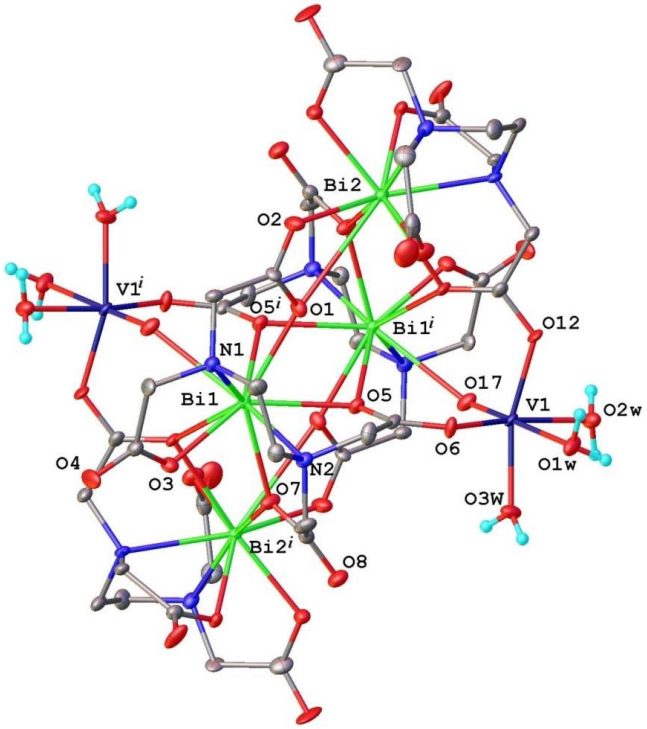

Figure 1. Structure of the hexanuclear molecular complex in the crystal structure of **1**. Thermal ellipsoids are drawn at 30% probability level. Non-relevant H-atoms and non-coordinated water molecules were omitted for clarity. Symmetry code: *i)* 1.5 – *x*, 0.5 - *x*, 1 - *z*

The hexanuclear aggregates in the crystal of **1** are associated through an extended system of intermolecular H-bonds where the water molecules are donors while the carboxylate oxygen

atoms act as acceptors. Accordingly, the crystal structure can be characterized as a three-dimensional supramolecular architecture (Fig. S1).

***[{VO(bpy)(H_2O)}$_2${Bi(edta)}$_4$]·30H_2O* (2)**. Addition of 2,2'-bipyridine to **1** gives rise to compound **2** but, surprisingly, does not change essentially the architecture of the hexametallic aggregates (Fig. 2). In the similar hexanuclear neutral units, the axial sites occupied by two water molecules in the coordination sphere of vanadium in **1** are taken by the nitrogen atoms of 2,2'-bipyridine in **2**. This modification is accompanied by bending of the O17-V1-O1*w* angle to 172.5(3)^o and to a slight distortion of the equatorial plane of vanadium coordination octahedron. The displacement of the vanadium atom from the mean equatorial plane towards the apical vanadyl oxygen is 0.231 Å. The V-N distances in **2** are consistent with the literature data.[42]

The coordination geometry around the Bi1 ions is very similar to the one found in complex **1,** while the Bi2 polyhedron is more distorted as a result of elongation of bridging Bi-O1 bond to 3.165(6) Å. The Bi1-O17-V1 angle (142.1(3)^o) is larger than its analogue in **1** but it is still in line with a sp^2 hybridization of the vanadyl oxygen. Similar to **1,** the crystal structure of **2** is built as a 3D supramolecular network based on intermolecular O-H···O hydrogen bonds (Fig. S2).

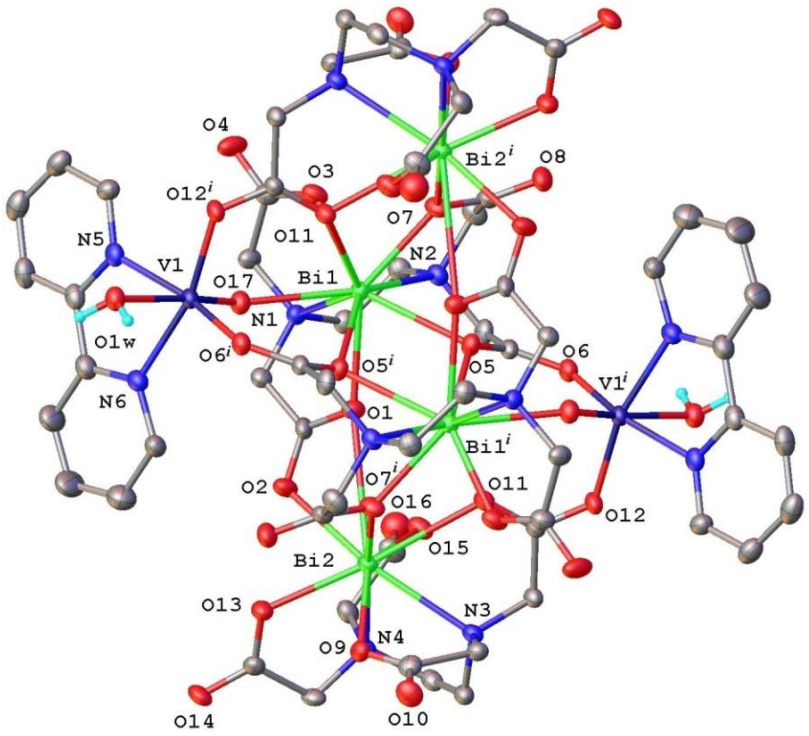

Figure 2. Structure of the hexanuclear molecular complex in the crystal structure of **2**. Thermal ellipsoids are drawn at 30% probability level. Non-relevant H-atoms and non-coordinated water molecules were omitted for clarity. Symmetry code: $^{i)}$ 1 - *x*, 1 - *y*, 1 – *z*

{[VO(H$_2$O)$_3${Bi(cdta)}$_2$]·7.7H$_2$O}$_n$ (**4**). The main structural unit of **4** is shown in Figure 3. These units are assembled into a two-dimensional coordination polymer (Fig. S3). Similar to **1** and **2**, the vanadium atom exhibits a slightly distorted octahedral environment. It is noteworthy, that in contrast to **1** and **2** the vanadyl oxygen in **4** is not coordinated to bismuth. The equatorial plane of the polyhedron is formed by three water molecules and by an oxygen atom of a bridging carboxylate group. The apical positions are occupied by a vanadyl oxygen atom at 1.63(1) Å and by the bridging carboxylate oxygen at a longer distance (V-O14 = 2.15(1) Å). The O17-V-O14 angle is 177.2(4)^{o}.

Surprisingly, the V=O bond length (1.63(1) Å) is longer in **4**, in which the vanadyl oxygen is not coordinated to bismuth, than in **1** (1.594(5) Å) and **2** (1.618(6) Å), where the V=O

forms coordination bonds with bismuth ions. Generally, vanadyl donation leads to an increase of V=O separation as a result of the diminution of the electron density on the vanadyl oxygen and supporting examples have been reported.[38c] This discrepancy could arise from the influence of the various oxygen donor atoms *trans*- to the vanadyl oxygen. As already mentioned, this site is occupied by water molecules in **1** and **2**, while in **4** the position is taken by an oxygen atom of a bridging carboxylate fragment. The displacement of vanadium from the mean equatorial plane of the coordination polyhedron in **4** is 0.247 A˚.

The coordination number of both Bi^{3+} ions in **4** is eight. The coordination polyhedra include the six donor atoms (2N+4O) of the *cdta*$^{4-}$ ligands and are completed by two symmetrically-related carboxylate oxygen atoms. The coordination polyhedra of Bi1 and Bi2 can be best described as distorted square antiprisms.

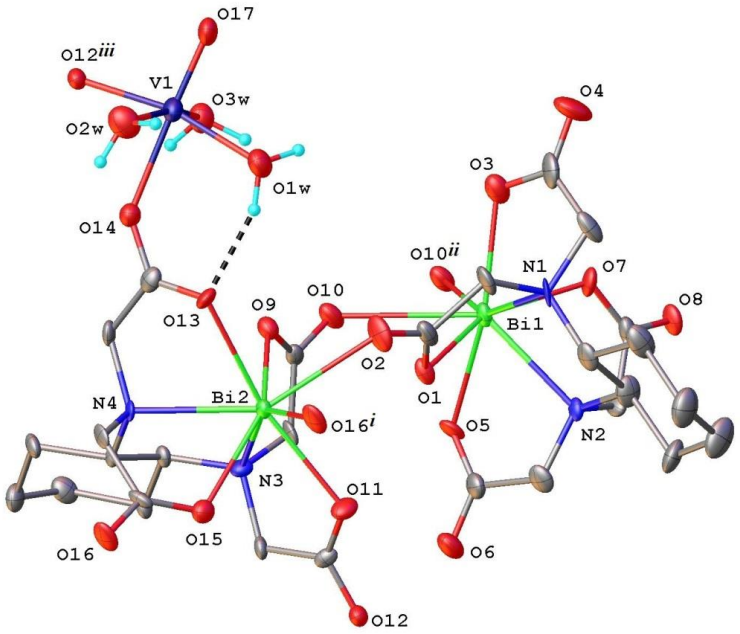

Figure 3. View of the asymmetric unit in the crystal structure of **4** with the thermal ellipsoids at 50% level. Non-relevant H-atoms and non-coordinated water molecules were omitted for clarity. Symmetry codes: [i] 2 – *x*, -*y*, 1 – *z*; [ii] 2 – *x*, 1 - *y*, -*z*; [iii] -1 + *x*, *y*, *z*

The coordination modes of the two crystallographically independent *cdta*$^{4-}$ ligands are different. Thus, the heptadentate ligand coordinated to Bi1 has one bidentate and three unidentate carboxylate groups while in the {Bi2(cdta)}$^{-}$ units there are three bidentate carboxylate and one tridentate-bridging groups. It is noteworthy that in the latter case the *cdta*$^{4-}$ ligand is undecadentate using all ten of its donor atoms (2N+8O) for coordination. Though it involves only eight atoms (2N+6O) in coordination, the *edta*$^{4-}$ ligand in the structure of **1** is also undecadentate (Fig. 1). This is the highest coordination capacity reported for Bi(III)-diaminetetracarboxylate-based complexes. In all the structurally studied Bi(III)-*edta* or Bi(III)-*cdta* compounds,[31] the ligands act as hexa-, hepta-, octadentate or, as recently published,[43] decadentate coordination agents.

***{[Cu(H$_2$O)$_2${Bi(cdta)(H$_2$O)}$_2$]·H$_2$O}$_n$* (5)**. The asymmetric unit of the crystal structure of **5** along with atom labeling scheme is shown in Figure 4. The octahedral coordination of copper ion, which occupies a special position on the center of symmetry, is performed by two water molecules and four oxygen atoms of the bridging carboxylate fragments. The apical Cu-O6 bond lengths (Table 2) give rise to a Jahn-Teller distortion around the Cu^{2+} ion. Similar to **4**, the bismuth ions in **5** displays a coordination number of eight which includes six atoms donated by the *cdta*$^{4-}$ ligands (2N+4O), one water molecule and a bridging carboxylate oxygen of a symmetry equivalent {Bi(cdta)(H$_2$O)$^{-}$} unit. The coordination polyhedron of Bi^{3+} ions is a distorted square antiprism, similar to that found in **4**. The asymmetric units of the structure are assembled via a center of inversion to form 1D polymeric coordination chains. These polymeric chains are associated through H-bonds with solvate water molecules resulting in the formation of a 3D supramolecular architecture (Fig. S4).

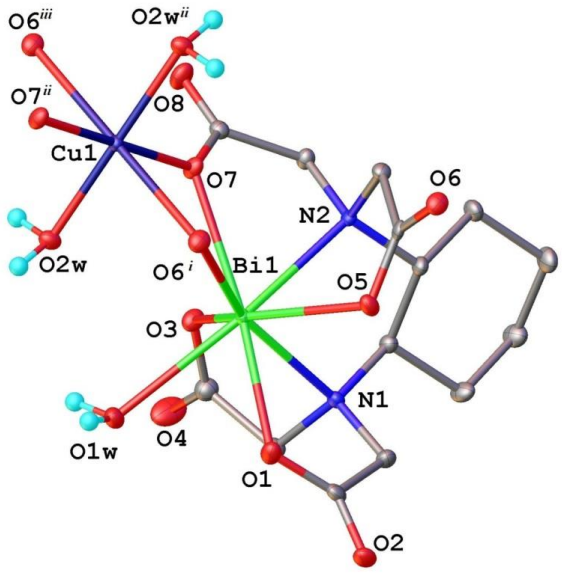

Figure 4. View of the asymmetric unit in the crystal structure of **5** with the thermal ellipsoids at 50% level. Non-relevant H-atoms and non-coordinated water molecules were omitted for clarity. Symmetry codes: ^{i} *–x, -y, –z*; ^{ii} -1 *– x, -y, -z*; ^{iii} -1 *- x, -y, -z*

The closest analogue of **5**, with respect to composition and crystal structure, is $[Cu(H_2O)_6][Bi(edta)]_2 \cdot 3H_2O$.[36] In both structures, aquated Cu^{2+} ions are intercalated between $Bi(APC)^-$ moieties but the aggregations are quite different. In **5**, $\{Cu(H_2O)_2\}^{2+}$ units assemble $\{Bi(cdta)(H_2O)\}^-$ moieties into 1D polymeric chains by means of both coordination and hydrogen bonds (Fig. S4). In the case of $[Cu(H_2O)_6][Bi(edta)]_2 \cdot 3H_2O$, $[Cu(H_2O)_6]^{2+}$ cations are connected to $[Bi(edta)^-\}_n$ polymeric chains only by hydrogen bonds.

IR spectroscopy. The variations observed in the position of bands attributable to COO sets in the IR spectra of the free carboxylic acids and corresponding metal complexes are indicative of the probable coordination mode of carboxylate groups.[44a] The bands due to carbon-oxygen stretching vibration, observed at 1751 - 1693 cm^{-1} for the non-coordinated H_4APC acids,

are shifted to 1670-1557 cm^{-1} (ν_{as}(COO)) in the title compounds (Table 3) as a result of coordination of COO groups to the metal centres.[44b]

Table 3. Assignments of vibration bands (cm^{-1}) from IR spectra of the complexes

Compound	ν_{as}COO	ν_sCOO	$\Delta(\nu_{as}-\nu_s)$	νC-N (APC)	ν(V=O)	ν C-C (CH_2COO) or (C_6H_{10})'
1	1562	1408 1380	154 182	1111 1086	958	914
2	1574	1404 1378	170 196	1109 1088	954	911
3	1575	1363	212	1092	973	915
4	1640 1557*	1388 1354	252(169*) 286(203*)	1099 1082	984	922, 936 880'
5	1670 1597*	1399 1376 1351	271(198*) 294(221*) 320(246*)	1092 1077		907, 923 875'

Considering $\Delta\nu = \nu_{as}(COO^-) - \nu_s(COO^-)$ differences[44c] in the spectra of the analyzed complexes, we can expect the bonding between the metal ions and the carboxylate groups to be dominantly bidentate or bidentate-bridging in case of compounds **1** and **2** ($\Delta\nu < 200\ cm^{-1}$)**,** while complexes **3-5** should display both unidentate and bidentate/bridging coordination modes of the carboxylate groups ($200\ cm^{-1} < \Delta\nu < 200\ cm^{-1}$). This observation agrees with the crystal structures of **4** and **5**.

The IR bands assigned to *ν*(V=O) appear in the range 954 - 984 cm^{-1}. This band is located at 984 cm^{-1} for complex **4**, which does not involve V=O in coordination (Fig. 3) and is shifted to 954 and 958 cm^{-1} for compounds **1** and **2,** where vanadyl is coordinated to bismuth (Fig. 1 and 2). The presence of non-coordinated vanadyl can be assumed in compound **3** as the *ν*(V=O) band has a value closer to that of **4** (Table 3).

Another band affected by coordination is ν(C-C) of -CH_2COO^- groups which is shifted from 947 cm^{-1} (H_4edta) and 965 cm^{-1} (H_4cdta) in the non-coordinated acids to 911-936 cm^{-1} in the complexes. The signals at 875 cm^{-1} and 880 cm^{-1} in the IR spectra of $cdta^{4-}$-based compounds **4** and **5** are tentatively assigned to ν(C-C) of cyclohexane ring.

Thermogravimetric analysis. The thermal decompositions of the precursors were followed by combined TG/DTA curves (Fig. 5, S5 and S6). The results are summarised in Table 4.

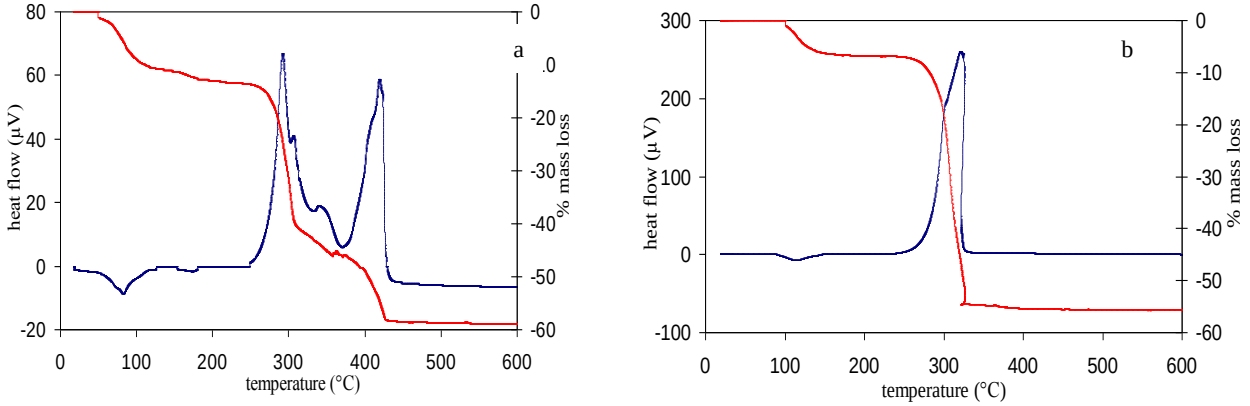

Fig. 5. TG and DTA curves of **4** (a) and **5** (b)

Generally, the decomposition of all the complexes occurs in several stages. The first process is endothermic and, depending on the precursor, takes place between 50 and 200 °C and corresponds to the elimination of water. This process occurs in two steps for precursors **2** and **4** or in three steps for **1** (Table 4) indicating the non-equivalent nature of the water in these compounds. This assumption is confirmed by their crystallographic data.

Table 4. TG/DTA study results

Compound	Dehydration max., ^{o}C	Ligand thermolysis, ^{o}C	Residual mass %, experim.(calcul.) (for $Bi_4V_2O_{11}$; Bi_2CuO_4)
1	80; 125; 170	280-450	48(44)
2	80; 130	240-420	38(37)
3	80	260-455	42(38)
4	85; 175	250-435	41(41)
5	115	245-330	44(43)

For instance, in case of **4**, the first step (Fig. 5a) corresponds to the release of the molecules of crystallisation water (10.0% weight loss vs 10.2% calculated). The second endothermic process is consistent with the elimination of the water molecules (3.4% weight loss vs 4.0% calculated) coordinated to vanadium in the equatorial plane of the octahedron, in good accordance with its crystal structure (Fig. 3). Moreover, a three-step elimination of the water molecules from compound **1** (Fig. S5) agrees well with its structural formula. The first process begins with the loss of the molecules of crystallization water (10.0% vs 12.0% calc.). The second endothermic effect corresponds to the release of the most distant (d V1-O1*w* = 2.174(5) Å) apical water molecules (Fig. 1) (1.6% vs 1.4% calc.), while the equatorial water molecules, which are coordinated at shorter distances (2.039(4) and 2.012(5) Å), are eliminated last on heating (2.8% weight loss vs 2.8% calc.).

The second decomposition stage of the complexes includes the oxidative degradation of APC and 2,2'-bipyridyl ligands, occurring for the vanadium-based precursors in two or three distinct successive exothermic effects in the 240-455 °C temperature range (Table 4). Interestingly, the elimination of the organic matrix for the copper-containing precursor proceeds in only one exothermic event accompanied by an abrupt mass loss (Fig. 5b). Even more, its

complete decomposition temperature is 105-130 ^{o}C lower than for the vanadium-based precursors.

Finally, the decomposition of the precursors ends in the formation of inorganic residues. The total weight loss is in relatively good agreement with the formation of the expected $Bi_4V_2O_{11}$ or Bi_2CuO_4 mixed-oxides (Table 4).

Temperature controlled X ray diffraction (TCXRD) studies. The analysis of thermal decomposition of the precursors has been completed by *in situ* TCXRD (Fig. 6, S7-S9) under static air at 10 ^{o}C·min^{-1} heating rate, trying to mirror the conditions from TG/DTA section. TCXRD performed in air flow or at lower heating rates or decompositions at different thermolysis conditions have been probed for comparison. Our goal was to analyze the factors in competition in order to identify the optimal conditions that would lead to the desired mixed-oxides in pure form. The effects of the ligands nature, of the intermetallic distances in the precursors, of the thermal treatment conditions (heating rate, annealing time) and of the gaseous atmosphere on the mixed-oxide formation process have been analyzed for this purpose.

Considerable effort has been previously made to control the stoichiometry of the heterometallic oxides resulting upon thermolysis of suitable molecular precursors. Generally, heating time and temperature have been the most frequently tested factors. Occasionally, the ligand nature[25,45] or the gaseous atmosphere[25] have been also probed. However, according to our recent findings the final product composition is strongly dependent upon the heating rate.

The TCXRD results of the precursors are summarised in Table 5. The degradation process under static air at 10 ^{o}C·min^{-1} heating rate provides the optimal reaction only in the case of precursors **1**, **2** and **5** since the final residues, after cooling to room temperature, are the expected pure $Bi_4V_2O_{11}$ or Bi_2CuO_4. Under the same experimental conditions, precursor **4** yields

a mixture of four oxides with significant amounts of the three undesired components (Fig. 6, Table 5).

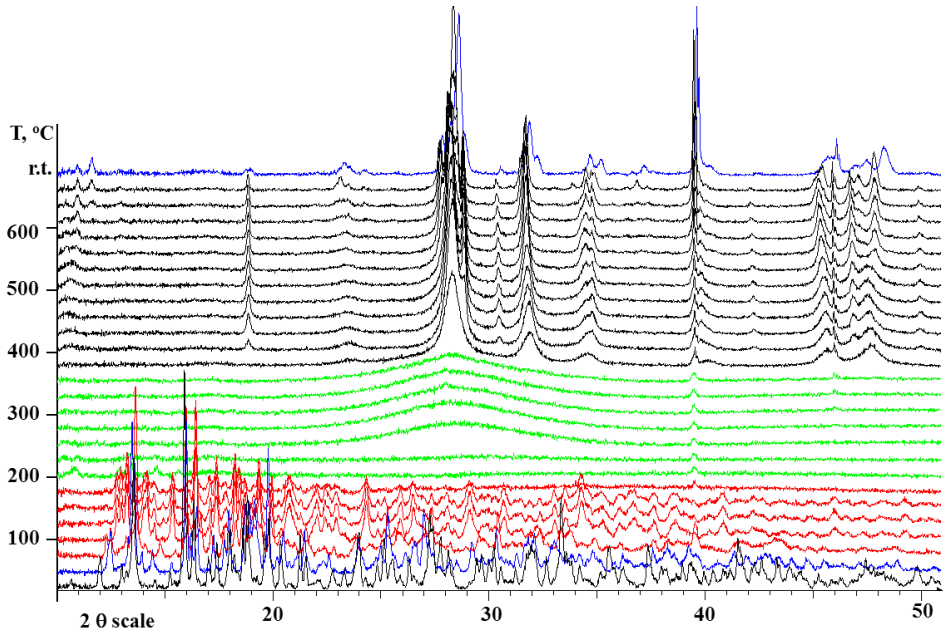

Fig. 6. TCXRD patterns of **4** recorded at 10 $^{o}C \cdot min^{-1}$ heating rate in static air. The top trace is the XRD pattern of the material cooled to room temperature.

When the decomposition of **4** was performed in air flow (5 $L \cdot h^{-1}$), the expected $Bi_4V_2O_{11}$ was formed by 250 ^{o}C, along with small amounts of $Bi_{11}VO_{19}$ and $BiVO_4$ (Table 5, Fig. S10). Not even annealing at 800 ^{o}C for 4 hours, after decomposition of **4** at a heating rate of 10 $^{o}C \cdot min^{-1}$ led to the formation of the pure $Bi_4V_2O_{11}$ mixed-oxide.

Table 5. TCXRD analysis results of the decomposition in static air at 10 $^{o}C \cdot min^{-1}$ heating rate unless otherwise specified (*w* = weak)

Precursor	Temperature, °C	Indexed oxide(s)	Final compounds after cooling to room temperature	Notes
1	350 – 375	$Bi_8V_2O_{17}$	$Bi_4V_2O_{11}$	
	400-525	$Bi_8V_2O_{17}$ + $BiVO_4$		
	550-625	$Bi_8V_2O_{17}$ + $BiVO_4$ + + $Bi_{11}VO_{19}$		
	650	$Bi_8V_2O_{17}$ + $BiVO_4$ + + $Bi_{11}VO_{19}$ + γ-$Bi_4V_2O_{11}$		
2	250-325	$Bi_{11}VO_{19}$	$Bi_4V_2O_{11}$	
	350	$Bi_{11}VO_{19}$ + $Bi_8V_2O_{17}$		
	375-625	$Bi_{11}VO_{19}$ + $Bi_8V_2O_{17}$ + + $BiVO_4$		
	650	$Bi_4V_2O_{11}$		
3	275-400	unknown phase	unknown phase	flowing air
	425-700	unknown phase + + $Bi_4V_2O_{11}$	$Bi_4V_2O_{11(w)}$	
			$Bi_4V_2O_{11}$ + + $Bi_{11}VO_{19(w)}$ + $BiVO_{4(w)}$	annealing for 4 h at 600 ^{o}C
4	375	$Bi_8V_2O_{17}$	$Bi_4V_2O_{11}$ + $Bi_8V_2O_{17}$ + + $Bi_{11}VO_{19}$ + $BiVO_4$	
	400-525	$Bi_8V_2O_{17}$ + $BiVO_4$		
	550-600	$Bi_8V_2O_{17}$ + $BiVO_4$ + + $Bi_{11}VO_{19}$		
	625-650	$Bi_8V_2O_{17}$ + $BiVO_4$ + + $Bi_{11}VO_{19}$ + $Bi_4V_2O_{11}$	$Bi_4V_2O_{11}$	3 $^{o}C \cdot min^{-1}$ heating rate, annealing for 1 h at 800 ^{o}C
4	250-650	$Bi_4V_2O_{11}$ + $Bi_{11}VO_{19(w)}$ + + $BiVO_{4(w)}$	$Bi_4V_2O_{11}$ + $BiVO_{4(w)}$	flowing air
	675-800	$Bi_4V_2O_{11}$ + $BiVO_4$		
4	350-500	$BiVO_4$	$Bi_4V_2O_{11}$	0.2 $^{o}C \cdot min^{-1}$ heating rate
	500-560	$BiVO_4$ + $Bi_{11}VO_{19}$		
	560-630	$BiVO_4$ + $Bi_{11}VO_{19}$ + + $Bi_4V_2O_{11}$		
	630-800	$Bi_4V_2O_{11}$		
5	250-350	$Bi_{7.38}Cu_{0.62}O_{11.69}$ + Bi_2O_3	Bi_2CuO_4	
	400-625	Bi_2CuO_4 + Bi_2O_3		
	650	Bi_2CuO_4		
5	340-800	Bi_2CuO_4	Bi_2CuO_4	0.2 $^{o}C \cdot min^{-1}$ heating rate

Notably, when the same precursor was thermally treated at a lower heating rate (3 $^{o}C \cdot min^{-1}$), followed by one hour of annealing, the final residue after cooling was pure $Bi_4V_2O_{11}$ (Table 5). Surprisingly, thermolysis of compound **3** even in flowing air leads to the formation of an unknown phase as the major crystalline product along with $Bi_4V_2O_{11}$ as a minor component (Fig. S11). The expected $Bi_4V_2O_{11}$ could be obtained as the main crystalline residue only after an additional four hours of annealing at 600^{o}C (Table 5).

A detailed analysis of the thermal degradation process of the vanadium-containing precursors under static air at a heating rate of 10 $^{o}C \cdot min^{-1}$ demonstrates that the appearance of $Bi_4V_2O_{11}$ mixed-oxide is generally preceded/accompanied by the formation of the $Bi_{11}VO_{19}$ phase. Thus, for complexes **1** and **4,** the gradual formation of $Bi_4V_2O_{11}$ starts with the appearance of $Bi_8V_2O_{17}$, followed by crystallization of $BiVO_4$, and later by $Bi_{11}VO_{19}$. A distinct feature of the decomposition of **2** is that the crystallization of the inorganic residue starts with $Bi_{11}VO_{19}$, which persists throughout the decomposition process until pure $Bi_4V_2O_{11}$ forms at 650 ^{o}C (Fig. S8).

Considering the similarity of the structures of **1** and **2** (Fig. 1 and 2), that have comparable short intermetallic V---Bi separations (3.955 Å and 3.916 Å), it appears that the presence of the *bpy* ligand is the main reason for the different order of appearance of the intermediates throughout its thermo-degradation pathway. As a result, pure $Bi_4V_2O_{11}$ is formed exclusively from **2** as the only crystalline material before the sample is cooled to room temperature (Table 5). It is most probable that *bpy*, which serves as additional combustible material (Table 6), brings a beneficial contribution to the mixed-oxide formation process. A similar situation was observed in the previously reported Ba-Co-APC precursors.[25] Among the

analyzed complexes, only the samples containing ~31-32 % carbon produced the desired single-phase 2H-$BaCoO_{3-\delta}$.

Table 6. Calculated C, H and N content of the anhydrous compounds

Compound	E %			
	C	H	N	C + N
$VO\{Bi(edta)\}_2$	22.63	2.28	5.28	27.91
$VO(bpy)\{Bi(edta)\}_2$	29.59	2.65	6.90	36.49
$VO(bpy)_2\{Bi(edta)\}_2$	34.97	2.93	8.16	43.13
$VO\{Bi(cdta)\}_2$	28.76	3.10	4.79	33.55
$Cu\{Bi(cdta)\}_2$	28.84	3.11	4.80	33.64
$Cu\{Bi(edta)\}_2$[33]	22.71	2.29	5.30	28.01
$VO(phen)_2\{Bi(edta)\}_2$[42]	37.17	2.84	7.88	45.05
$V(acac)_3Bi_2(Hsal)_6$[23e]	42.92	3.60	-	42.92
$[BiCl_3OV(OC_2H_4OCH_3)_3]_2$[32]	17.79	3.48	-	17.79

One can consider the carbon amount in the precursors as a tool for controlling the residue composition. A higher carbon percentage (~34% for **3**) requires more rigid thermal conditions to generate the desired $Bi_4V_2O_{11}$ mixed-oxide (Table 5). Moreover, a further increase in the carbon content to over 37% (Table 6) eventually can result in reduction of Bi(III) ions to metallic bismuth, as observed in the case of the thermal decomposition of $VO(phen)_2\{Bi(edta)\}_2{\cdot}5H_2O$ in static air. [46] Notably, the reported molecular precursors $V(acac)_3Bi_2(Hsal)_6$[23e], which contains a considerably higher amount of carbon (42.92%), and $[BiCl_3OV(OC_2H_4OCH_3)_3]_2$[32], which contains a much lower ratio of carbon (17.79%), do not yield the expected $Bi_4V_2O_{11}$ or $BiVO_4$ in pure form.

The formation of the final single-phase residues for the *edta*$^{4-}$-based samples **1** and **2**, when compared to their *cdta*$^{4-}$ analogue **4**, is assumed to be favored by a closer separation of the heterometallic species in these precursors. Thus, the shortest Bi---V distance in **4** is 5.716 Å,

while in **1** and **2** these separations are reduced to 3.955 Å and 3.916 Å. Accordingly, this might facilitate a more intimate mixing of the different metals during decomposition stage.

Confirmation of the influence of heating rate on the mixed-oxide formation process is found in the TCXRD patterns of **4** (Fig. 7) and **5** (Fig. S12) recorded during thermal decomposition in static air at a much lower (0.2 $^{o}C \cdot min^{-1}$) heating rate. As demonstrated by the Guinier-Lenne pattern of **4**, the expected $Bi_4V_2O_{11}$ starts to crystallize at a lower temperature (560 ^{o}C vs 625 ^{o}C) and is obtained as the only detected residue by 630 ^{o}C, in contrast to a mixture of four phases at 10 $^{o}C \cdot min^{-1}$ for the same precursor (Table 5).

A similar situation was observed in the Guinier-Lenne pattern of **5** where the target Bi_2CuO_4 was detected in pure form by 340 ^{o}C at 0.2 $^{o}C \cdot min^{-1}$ heating rate versus 650 ^{o}C at 10 $^{o}C \cdot min^{-1}$ (Table 5). Notably, the temperature of appearance of bismuth cuprate from **5** is 20 ^{o}C lower than found from the TCXRD pattern of the analogous precursor with $edta^{4-}$, namely $Cu[Bi(edta)]_2 \cdot 9H_2O$.[36] Here one should note the influence of the APC ligand, which affects the carbon content (Table 6) and, most probably, of the intermetallic distances from the initial precursor on the mixed-oxide formation. Surprisingly, when **5** is decomposed at a much higher heating rate (20 $^{o}C \cdot min^{-1}$), followed by two hours of annealing, the final crystalline product is mainly $Bi_{7.38}Cu_{0.62}O_{11.69}$ (Fig. S13). The expected Bi_2CuO_4 is present at only low amounts.

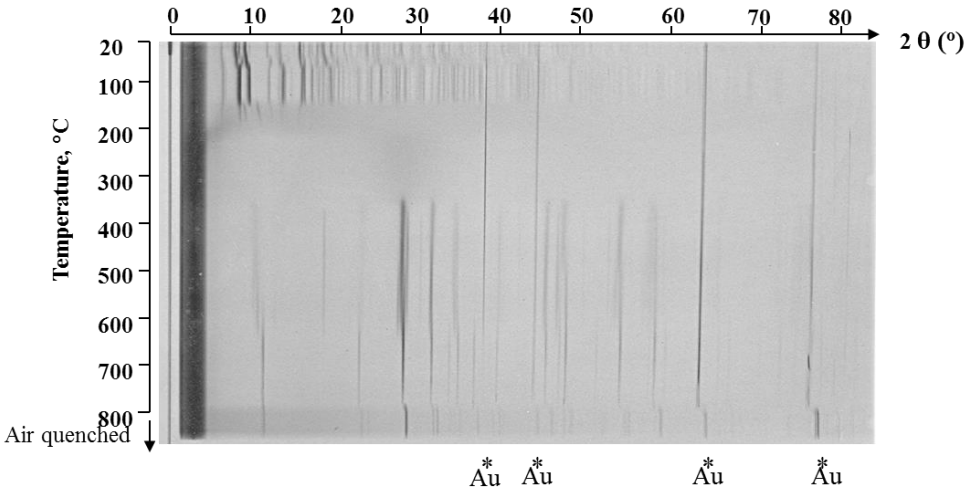

Fig. 7. Guinnier-Lenne pattern of **4** recorded at 0.2 $^{o}C \cdot min^{-1}$ heating rate in static air

Several attempts to obtain $Bi_4V_2O_{11}$ via various synthetic methods have been reported by other authors. Generally, high temperatures and long times were used in the preparation process and the desired product was frequently accompanied by $BiVO_4$. Sometimes Bi_2O_3 or unknown impurities were also indexed in the final residues (Table S1).

The advantage of aminopolycarboxylate SSMP method to access heterobimetallic oxides is clearly demonstrated since pure $Bi_4V_2O_{11}$ or Bi_2CuO_4 can be easily obtained by slow heating of the appropriate heterometallic complexes to moderate temperatures. Most likely, slower heating of the molecular precursors, where the different metals are *a priori* uniformly distributed at an atomic scale, facilitates optimal reactions between the metallic centres. This prevents metal segregation and favours the formation of the expected stoichiometric mixed-oxides at temperatures even lower compared to the successful attempts performed at higher heating rates.

Microstructural properties. The SEM images of the powders resulting after heating the samples to 650 ^{o}C confirm the presence of porous agglomerates with sizes within 1-70 μm range depending on the starting precursor (Fig. 8). The agglomerates are formed of strongly

interpenetrated spherical or ellipsoidal grains with sizes within 0.3-3 μm range, the smallest grains being present in the residues produced by the *cdta*$^{4-}$-based precursors. The presence of numerous pores and channels permeating the oxide materials (Fig. 9) is most probably due to the abundant gaseous products released during oxidative destruction of the organic matrix from the complexes.

The results clearly demonstrate that for both vanadium and copper *cdta*$^{4-}$ complexes, the removal of the organic species generates final residues of a rather homogeneous morphology. A similar situation was found in case of the *bpy-edta*$^{4-}$-based precursor **2**, though the grain agglomerates are slightly larger. The most heterogeneous morphology of the residue was obtained for the *edta*$^{4-}$-containing precursor **1**.

The difference in the morphology and grain size of the oxide material was related to the amount of combustible material in the precursors (Table 6). It appeared that compound **1**, with the smallest carbon content, leads to the largest and most heterogeneous grain agglomerates of the residue, while the *cdta*$^{4-}$-based precursors **4** and **5**, along with *bpy-edta*$^{4-}$-precursor **2** having higher and close carbon percentages, eventually yield smaller grains and more homogeneous morphology of the residues.

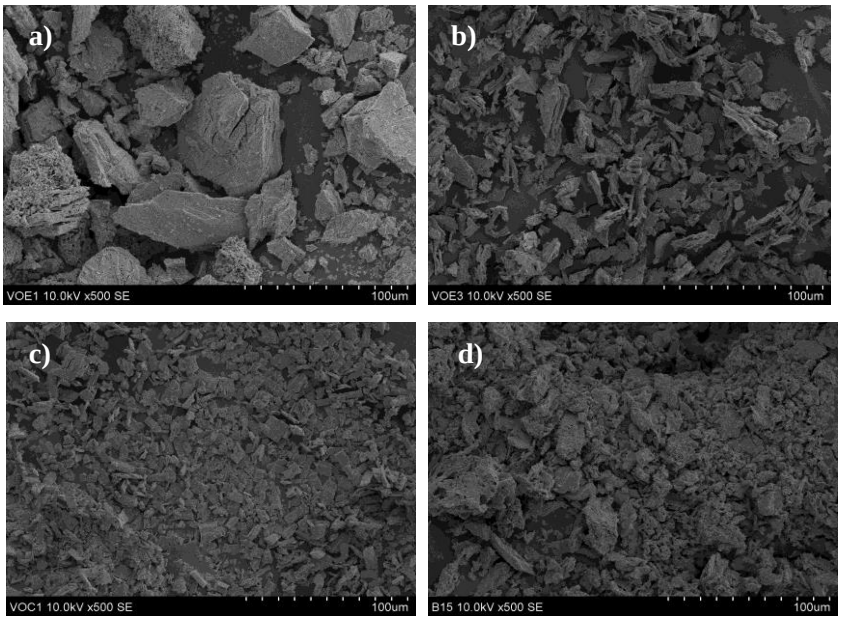

Fig. 8. SEM images of the residues produced after thermal treatment to 650 ^{o}C of **1** (a), **2** (b), **4** (c) and **5** (d) (magnification ×500)

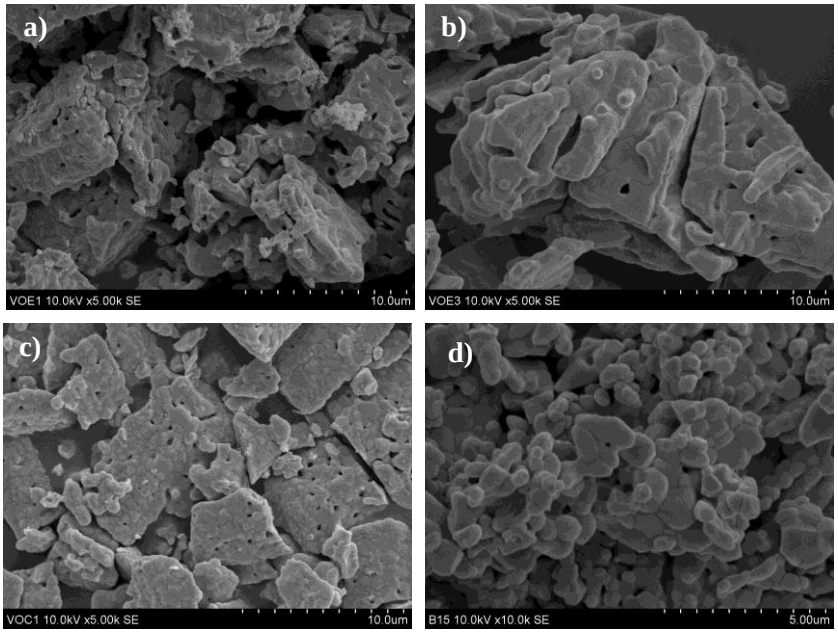

Fig. 9. SEM images of the residues produced after thermal treatment to 650 ^{o}C of **1** (a), **2** (b), **4** (c) (magnification ×5000) and **5** (d) (magnification ×10000)

This is consistent with results reported for the precursor **5** homologue $Cu\{Bi(edta)\}_2 \cdot 9H_2O$[36] with smaller carbon content in the anhydrous compound (22.71% vs

28.84% in **5**), which yielded upon thermolysis grains of about 1 μm, compared to 0.3-1 μm in case of **5**. This is in line with our previous studies based on Ba-Co-APC system that confirmed a rather homogeneous distribution of spherical particles of about 50 nm only in the samples derived from Ba-Co-*cdta*$^{4-}$ precursors (%C = ~31-32)].[25] Under the same experimental conditions, Ba-Co-*edta*$^{4-}$ or Ba-Co-*nta*$^{3-}$ analogues (%C = ~21-26) produced needles and platelets with sizes from 0.5 to 3 microns long.

CONCLUSIONS

The use of APC-based single source molecular precursors is able to overcome some of the drawbacks of traditional solid state synthetic routes to heterometallic bismuth oxides, in particular poor control of the stoichiometry and homogeneity of the resulting oxide materials. The heterometallic compounds formed by this method were found to smoothly decompose under thermolysis to produce mixed-oxides. The composition of the APC molecular precursors can be easily adjusted by using appropriate aminopolycarboxylates or additional ligands to achieve an optimal amount of combustible material as observed empirically, although the exact explanation for why the amount of carbon is important could derive from a variety of possible explanations such as the amount of gaseous products or some indirect control over the kinetics of the reactions. It seems likely that the cumulative effect of short intermetallic separations and appropriate amount of combustible material from the precursors combined with low heating rates, acting in concert, are what ultimately produce the pure heterometallic oxides. The conditions required to produce these oxide materials from the molecular precursors reported here are significantly milder than what has been previously reported, opening up the possibility of preparing new metastable bismuth mixed-oxides. The differences observed in terms of grain size and morphology between the analyzed residues supports the postulate that the nature of the

initial organic ligands essentially affects the microstuctural properties of the final bimetallic oxides.

ASSOCIATED CONTENT

Supporting Information. Additional structure figures of **1**, **2**, **4** and **5**; TG/DTA curves for **1** and **3**; TCXRD patterns of **3** and **4**, XRD pattern of **5** (PDF). X-ray crystallographic file (CIF) for **1**, **2**, **4** and **5**. This material is available free of charge via the Internet at http://pubs.acs.org.

ACKNOWLEDGEMENT

This work has been carried out with the financial support of Project 10.820.05.22/RoF and the Robert A. Welch Foundation (C-0976). I.B. gratefully acknowledges the Fulbright Fellowship ID 68130074.

REFERENCES

1. Eerenstein, W.; Mathur, N. D.; Scott, J. F. *Nature*, **2006**, *442*, 759.
2. *(a)* Park, B. H.; Kang, B.S.; Bu, S. D.; Noh, T.W.; Lee, J.; Jo, W. *Nature*, **1999**, *401*, 682; *(b)* Paz de Araujo, C.A.; Cuchiaro, J. D.; McMillan, L.D.; Scott, M.C.; Scott, J.F. *Nature*, **1995**, *374*, 627; *(c)* Scott, J. F.; Paz de Araujo, C. A. *Science*, **1989**, *246*, 1400; *(d)* Watanabe, T.; Funakubo, H.; Mizuhira, M.; Osada, M. *J. Appl. Phys.*, **2001**, *90*, 6533.
3. *(a)* Maeda, H. *Materia*, **2001**, *40*, 947; Maeda, H.; Tanaka, Y.; Fukuyama, M.; Asano, T. *Jpn. J. Appl. Phys*., **1988**, *27*, L209; *(c)* Rao, C. N. R.; Raveau, B. *Acc. Chem. Res.*, **1989**, *22*, 106; *(d)* Giannini, E.; Clayton, N.; Musolino, N.; Gladyshevskii, R.; Flukiger, R. *Front. Superconduct. Mater.*, **2005**, 739.
4. Sammes, N. M.; Tompsett, G.A.; Nafe, H.; Aldinger, F. *J. Eur. Ceram. Soc.*, **1999**, *19*, 1801.
5. *(a)* Arbosa, M.C.; Frejlich, J. *Trends in Optics and Photonics*, **2003**, *87*, 8731; *(b)* Blasse, G.; Ho, O. B. *J. Lumin.*, **1980**, *21*, 165; *(c)* Volkov, V. V.; Egorycheva, A. V. *Opt. Mater.*, **1996**, *5*, 273.
6. *(a)* Grasselli, R. K.; Burrington, J. D. *Adv. Catal.*, **1981**, *30*, 133; *(b)* Hanna, T. A. *Coord. Chem. Rev.*, **2004**, *248*, 429.
7. *(a)* Zou, Z. G.; Ye, J. H.; Sayama, K.; Arakawa, H. *Chem. Phys. Lett.*, **2001**, *343*, 303; *(b)* Tang, J. W.; Zou, Z. G.; Ye, J. H. *Angew. Chem. Int. Ed.*, **2004**, *43*, 4463; *(c)* Kim, H. G.; Hwang, D.W.; Lee, J. S. *J. Am. Chem. Soc*., **2004**, *126*, 8912.
8. Wienand, H.; Adel, J. in: G. Buxbaum (Ed.), *Industrial Inorganic Pigments*, Wiley-VCH, Weinheim, 1998.
9. Rohr, O. *Ind. Lubr. Tribol.*, **2002**, *54*, 153.

10. *(a)* Abraham, F.; Debreuille-Gresse, M. F.; Mairesse, G.; Nowogrocki, G. *Solid State Ionics*, **1988**, *28-30*, 529; *(b)* Vannier, R. N.; Pernot, E.; Anne, M.; Isnard, O.; Nowogrocki, G.; Mairesse, G. *Solid State Ionics*, **2003**, *157*, 147.

11. *(a)* Prasad, K. V. R.; Varma, K. B. R. *J. Phys. D: Appl. Phys.*, **1991**, *24*, 1858; *(b)* Ramasesha, S. K.; Singh, A. K.; Varma, K. B. R. *Mater. Chem. Phys*., **1997**, *48*, 136; *(c)* Alga, M.; Wahbi, M.; Ammar, A.; Tanouti, B.; Grenier, J. C.; Reau, J. M. *J. Alloys Compds.*, **1997**, *256*, 234; *(d)* Shantha, K.; Subbanna, G. N.; Varma, K. B. R. *J. Solid State Chem.*, **1999**, *142*, 41; *(e)* Arroyo y de Dompablo, M. E.; Moran, E.; Garcia-Alvarado, F. *Int. J. Inorg. Mater.*, **1999**, *1*, 83; *(f)* Shantha, K.; Varma, K. B. R. *Mater. Res. Bull.*, **1997**, *32*, 1581.

12. *(a)* Abraham, F.; Boivin, J. C.; Mairesse, G.; Nowogrocki, G. *Solid State Ionics* **1990**, *40-41*, 934; *(b)* Ueda, W.; Chen, C.-L.; Asakawa, K.; Moro-Oka, Y.; Ikawa, T. *J. Catal*., **1986**, *101*, 369; *(c)* Porta, P.; Lo Jacono, M.; Valigi, M.; Minelli, G.; Anichini, A.; De Rossi, S.; Gazzoli, D. *J. Catal*., **1986**, *100*, 86.

13. *(a)* Michel, C.; Hervieu, M.; Borel, M.M.; Gradin, A.; Deslandes, F.; Provost, J.; Raveau, B. *Z. Phys. B*, **1987**, *68*, 421; *(b)* Maeda, H.; Takaka, T.; Fukutomi, M.; Asano, T. *Jpn. J. Appl. Phys.*, **1988**, *27*, L209; *(c)* Leonyuk, A. L.; Babonas, G. J.; Szymczak, R.; Maltsev, V.; Shvanskaya, L.; Reza, A. *Physica C*, **2000**, *337*, 256; *(d)* Leyva, G.; Acha, C.; Levy, P.; Polla, G.; De Benyacar. M. A. R. *Progress High Temp. Supercond.*, **1990**, *25*, 626.

14. *(a)* Zhang, W.; Wang, R.; Liang, Y. *Beijing Chemical Institute: China*, 1996; *(b)* White, J. H. *Electric Power Research Institute: USA*, 1999.

15. *(a)* Gopalakrishnan, J. *Chem. Mater.*, **1995**, *7*, 1265; *(b)* Tokunaga, S.; Kato, H.; Kudo, A. *Chem. Mater.*, 2001, **13**, 4624; *c)* Hubert-Pfalzgraf, L. G. *Inorg. Chem. Commun.*, **2003**, *6*,

102; *d)* Neves, M. C.; Trindade, T. *Thin Solid Films*, **2002**, *406*, 93; *e)* Zhang, S.; Zhang, C.; Man, Y.; Zhu, Y. *J. Solid State Chem.*, **2006**, *179*, 62.

16. Barreca, D.; Depero, L. E.; Di Noto, V.; Rizzi, G. A.; Sangaletti, L.; Tondell, E. *Chem. Mater.*, **1999**, *11*, 255.
17. Lisoni, J. G.; Millan, P.; Vila, E.; Martın de Vidales, J. L.; Hoffmann, T.; Castro, A. *Chem. Mater.*, **2001**, *13*, 2084.
18. *(a)* Beale, A. M.; Sankar, G. *Chem. Mater.*, **2003**, *15*, 146; *b)* Liu, J. B.; Wang, H.; Hou, Y. D.; Zhu, M. K.; Yan, H.; Yoshimura, M. *Nanotechnology*, **2004**, *15*, 777.
19. Kim, Y.; Chae, H. K.; Lee, K. S.; Lee, W. I. *J. Mater. Chem.*, **1998**, *8*, 2317.
20. Tolstoy, V. P.; Tolstobrov, E.V. *Solid State Ionics*, **2002**, *151*, 165.
21. Veith, M. *J. Chem. Soc. Dalton Trans.*, **2002**, 2405.
22. *(a)* Mehring, M. *Coord. Chem. Rev.*, 2007, **251**, 974; *(b)* Ould-Ely, T.; Thurston, J. H.; Whitmire, *C* K. H.. *R. Chimie*, **2005**, *8*, 1906.
23. *(a)* Parola, S.; Papiernik, R.; Hubert-Pfalzgraf, L. G.; Jagner, S.; Hakansson, M. *J. Chem. Soc., Dalton Trans.*, **1997**, 4631; *(b)* Thurston, J. H.; Whitmire, K. H. *Inorg. Chem.*, **2002**, *41*, 4194. *(c)* Thurston, J. H.; Whitmire, K. H. *Inorg. Chem.*, **2003**, *42*, 2014; *(d)* Thurston, J. H.; Whitmire, K. H. *Chem. Mater.*, **2003**, *15*, 4407; *(e)* Thurston, J. H.; Trahan, D.; Ould-Ely, T.; Whitmire, K. H. *Inorg. Chem.*, **2004**, *43*, 3299; *(f)* Thurston, J. H.; Kumar, A.; Hofmann, C.; Whitmire, K. H. *Inorg. Chem.*, **2004**, *43*, 8427; *(g)* Whitmire, K. H.; Hoppe, S.; Sydora, O.; Jolas, J. L.; Jones, C. M. *Inorg. Chem.*, **2000**, *39*, 85; *(h)* Wójcik, K. *Dr. Thesis*, 2010, http://archiv.tu-chemnitz.de/pub/2010/0071.
24. Scurtu, R.; Somacescu, S.; Calderon-Moreno, J. M.; Culita, D.; Bulimestru, I.; Popa, N.; Gulea, A.; Osiceanu, P. *J. Solid State Chem.*, **2014**, *210*, 53.

25. Bulimestru, I.; Mentre, O.; Tancret, N.; Rolle, A.; Djelal, N.; Burylo, L.; Cornei, N.; Popa, N.; Gulea, A. *J. Mater. Chem.*, **2010**, *20*, 10724.

26. CrysAlis RED, Oxford Diffraction Ltd.,Version 1.171.36.32, 2003.

27. Dolomanov, O. V.; Bourhis, L. J.; Gildea, R. J.; Howard, J. A. K.; Puschmann, H. *J. Appl. Cryst.*, **2009**, *42*, 339.

28. Sheldrick, G.M. SHELXS, *Acta Cryst.*, **2008**, *A64*, 112.

29. Summers, S. P.; Abboud, K. A.; Farrah, S. R.; Palenik, G. J. *Inorg. Chem.*, **1994**, *33*, 88.

30. Wullens, H.; Devillers, M.; Tinant, B.; Declercq, J.-P. *J. Chem. Soc., Dalton Trans.*, **1996**, 2023.

31. Stavila, V.; Davidovich, R. L.; Gulea, A.; Whitmire, K. H. *Coord. Chem. Rev.*, **2006**, *250*, 2782.

32. Pell, J. W.; Davis, W. C.; zur Loye, H. C. *Inorg. Chem.*, **1996**, *35*, 5754.

33. Tucher, J.; Nye, L.; Ivanovic-Burmazovic, I.; Notarnicola, A.; Streb, C. *Chem. Eur. J.* **2012**, *18*, 10949.

34. Drewes, D.; Limanski, E. M.; Piepenbrink, M.; Krebs, B. *Z. Anorg. Allg. Chem.* **2004**, *630*, 58.

35. Botar, B.; Yamase, T.; Ishikawa E. *Inorg. Chem. Commun.* **_2000**, *3*, 579.

36. Sobanska, S.; Wignacourt, J.-P.; Conflant, P.; Drache, M.; Bulimestru, I.; Gulea, A. *Eur. J. Solid State Inorg. Chem.*, **1996**, *33*, 701.

37. Dikarev, E.; Zhang, H.; Li, Bo. *J. Am. Chem. Soc*. **2005**, *127*, 6156.

38. *(a)* Cashin, B.; Cunningham, D.; Gallagher, J. F.; McArdle, P.; Higgins, T. *J. Chem. Soc., Chem. Commun*., **1989**, 1445; (*b)* Choudhary, N. F.; Hitchcock, P. B.; Leigh, G. J.; Ng, S. W.

Inorg. Chim. Acta, **1999**, *293*, 147; *(c)* Cashin, B.; Cunningham, D.; Daly, P.; McArdle, P.; Munroe, M.; Chonchubhair, N. N. *Inorg. Chem.*, **2002**, *41*, 773.

39. Du, S. Z.; Feng, J.; Cheng, Y. F.; An, L.; Lu, X. M. *Z. Anorg. Allg. Chem.*, **2012**, *638*, 411.
40. *a)* Garcia-Jaca, J.; Insausti, M.; Cortes, R.; Rojo, T.; Pizarro, J. L.; Arriortua, M. I. *Polyhedron*, **1994**, *13*, 357; *b)* Arion, V. B.; Kravtsov, V. Ch.; Goddard, R.; Bill, E.; Gradinaru, J. I.; Gerbeleu, N. V.; Levitschi, V.; Vezin, H.; Simonov, Y. A.; Lipkowski, J.; Belskii, V. K. *Inorg. Chim. Acta*, **2001**, *317*, 33.
41. *a)* Selbin, J. *Chem. Rev.*, **1965**, *42*, 153; *b)* Selbin, J. *Coord. Chem. Rev.*, **1966**, *1*, 293; *(c)* Kahn, A.; Livage, J.; Collongues, R. *Phys. Status Solidi (A)* **1974**, *26*, 175; *d)* del Rio, D.; Galindo, A.; Vicente, R.; Mealli, C.; Ienco, A.; Masi, D. *J. Chem. Soc., Dalton Trans.*, **2003**, 1813.
42. *a)* Yang, W.; Lu, C. *Inorg. Chem*., **2002**, *41*, 5638; *b)* Triantafillou, G. D.; Tolis, E. I.; Terzis, A.; Deligiannakis, Y.; Raptopoulou, C. P.; Sigalas, M. P.; Kabanos, T. A. *Inorg. Chem*., **2004**, *43*, 79.
43. Stavila, V.; Gulea, A.; Popa, N.; Merbah, A.; Shova, S.; Simonov, Iu. A.; Lipkowski, J. *Inorg. Chem. Commun*., **2004**, *7*, 634.
44. *(a)* Bellamy, L. J. in: *The Infrared Spectra of Complex Molecules*, 3rd Edition, Chapman and Hall, London, **1975**, *288*, 183; *(b)* Nakamoto, K. in: *Infrared Spectra of Inorganic and Coordination Compounds*, 5th ed., John Wiley & Sons, New York, 1987; *(c)* Deacon, G. B.; Phillips, R. J. *Coord. Chem. Rev.*, **1980**, *33*, 227.
45. Boulmaaz, S.; Papiernik, R.; Hubert-Pfalzgraf, L. G.; Septea, B.; Vaissermann, J. *J. Mater. Chem.*, **1997**, *7*, 2053.

46. Bulimestru, I.; Wignacourt, J.-P.; Vannier, R.-N.; Drache, M.; Gulea, A. *The XXIX-th Romanian Chemistry Conference*, Calimanesti-Caciulata, Valcea, Romania, **2006**, Book of abstracts, 156.
47. Huve, M.; Vannier, R. N.; Nowogrocki, G.; Mairesse, G.; Van Tendeloo, G. *J. Mater. Chem.*, **1996**, *6*, 1339.
48. Castro, A.; Millan, P.; Ricote, J.; Pardo, L. *J. Mater. Chem.*, **2000**, *10*, 767.
49. Rullens, F.; Laschewsky, A.; Devillers, M. *Chem. Mater.*, **2006**, *18*, 771.
50. Chen, X.; Liu, J.; Wang, H.; Ding, Y.; Sun, Y.; Yan, H. *J. Mater. Chem. A*, **2013**, *1*, 877.
51. Pell, J. W.; Ying, J.Y.; zur Loye, H. C. *Materials Letters*, **1995**, *25*, 157.